INSTITUTE OF PLASMA PHYSICS

NAGOYA UNIVERSITY

RESEARCH REPORT

NAGOYA, JAPAN

Microwave Radiation from a Plasma in a Magnetic Field *

Shigetoshi TANAKA, Kenji MITANI **
and Hiroshi KUBO **

I P P J - 1 3 JULY 1963

Further communication about this report is to be sent to the Research Information Center, Institute of Plasma Physics, Nagoya University, Nagoya, JAPAN.

** Permanently at Yoshida College, Kyoto University, Sakyo-ku, Kyoto.

* This preliminary work was previously reported in Kakuyugo-Kenkyu 9 (1962) 188 (in Japanese).

ABSTRACT

The microwave radiations from a dc discharge plasma in a magnetic field were studied. The experimental results showed that the resonant radiations of the extraordinary wave, propagating perpendicular to a magnetic field, were observed not only at $\omega = (\omega_p^2 + \omega_b^2)^{1/2}$, but also near the cyclotron harmonics. On the other hand, it was shown that the dispersion relation for the plasma type oscillations derived by Bernstein had a harmonic structure: In our experimental condition their dispersion curve was divided into many branches, each of which approched asymptotically to the curves given by $\omega^2 = \omega_p^2 + \omega_b^2$ and by $\omega = n\,\omega_b$ (n being an integer). The resonant radiation detected was interpreted as the plasma type radiation, above mentioned. The gaps in the radiation spectrum at the cyclotron harmonics were not measured in our discharge plasmas. Further, the number of the successive harmonics in a radiation increased with decreasing the gas pressure, independently of the kind of gas used.

§ 1 Introduction

In this paper, the harmonic structure in the plasma oscillation is investigated by measuring the microwave radiations from a magnetoactive plasma.

As well known, the rf electromagnetic waves propagating in a magnetoactive plasma have two normal waves; ordinary and extraordinary[1]. If the thermal motion of plasma electrons is neglected, the extraordinary wave, propagating perpendicular to a magnetic field B, resonates at

$$\omega^2 = \omega_p^2 + \omega_b^2 \quad , \tag{1}$$

where $\omega_p = (ne^2/m\varepsilon_0)^{1/2}$ is the plasma frequency, $\omega_b = eB/m$ and ω the resonant frequency. Considering an effect of spatial dispersion in plasmas, the theoretical investigations on the plasma oscillations have been made extensively by many researchers [2)3)]. Bernstein [4)] has demonstrated that for longitudinal electron oscillations in this case, there are gaps in the spectrum of allowed frequencies at multiples of the electron cyclotron frequency, but zero Landau damping.

On the other hand, by the measurements on the microwave radiation from or absorption by a rather tenuous plasma in a magnetic field, the plasma type radiation, having the dispersion relation given in Eq. (1), has been observed by a number of workers [5)-8)]. It was reported also by Kato [9)] that the oscillations of two types were detected by a probe: the P-type oscillation given by Eq.(1) and the C-type oscillation given by $\omega = eB/m$. Further, the resonant radiations at the successive cyclotron harmonics, given by

$$\omega = n\omega_b \qquad (n = 1, 2, \cdots\cdots\cdots\cdots), \tag{2}$$

have been observed experimentally,[10) 11) 12)] although their physical

mechanism was not clear.

In the present experiments, the microwave radiations from an optically dense as well as tenuous plasma in a magnetic field are measured [13]. It is found that the plasma type radiation has the harmonic structure, which can be interpreted from the dispersion relation given by Bernstein.[4]

It has been reported[14] that very intense radiation due to the negative absorption effect at the cyclotron resonance was observed in slightly ionized gases such as Xe, Kr and Ar when the whole discharge tube was placed in a magnetic field. Such an anomalous radiation is not detected, however, in this work where a part of the positive column is immersed in a magnetic field. In the following, the procedures and the results of our experiments will be described in detail. Further, the harmonic structure of the dispersion relation will be investigated and the discussions will be given.

§ 2 Dispersion Relation

Since the measurements are made usually with varying magnetic field at the fixed frequency of rf wave, the dispersion relation will be re-examined from this point of view. The dispersion equation for an extraordinary wave, propagating perpendicular to a magnetic field $\vec{B}$, is given by [1]

$$k^2 \varepsilon_{zz} - \frac{\omega^2}{c^2} (\varepsilon_{xx} \varepsilon_{zz} - \varepsilon_{xz} \varepsilon_{zx}) = 0 , \qquad (3)$$

where $\vec{k}$ is the wave vector of propagating wave. Here, the z – and y–axis coincide with $\vec{k}$ and $\vec{B}$ respectively. Considering the effect of the spatial dispersion in plasmas, the components of dielectric permittivity tensor ε_{ik} are [15]

$$\left.\begin{aligned} \varepsilon_{xx} &= 1 + \frac{1}{4}(A - 2B + C)\,, \\ \varepsilon_{zz} &= 1 + \frac{1}{4}(A + 2B + C)\,, \\ \varepsilon_{zx} &= -\varepsilon_{xz} = \frac{i}{4}(A - C) \end{aligned}\right\} \tag{4}$$

and

$$\left.\begin{aligned} A(k,\omega) &= C(k,-\omega) = \frac{2\omega_p^2}{\omega\omega_b} \sum_{n=-\infty}^{\infty} \{\zeta_{n-1}(\lambda) + \lambda\zeta'_{n-1}(\lambda)\}\{n - \frac{\omega}{\omega_b}\}^{-1}\,, \\ B(k,\omega) &= \frac{2\omega_p^2}{\omega\omega_b}\lambda \sum_{n=-\infty}^{\infty} \zeta'_n(\lambda)(n - \frac{\omega}{\omega_b})^{-1}\,, \end{aligned}\right\} \tag{5}$$

where

$$\zeta_n(\lambda) = e^{-\lambda} I_n(\lambda)\,,$$

I_n : Bessel function of 1st kind of imaginary argument,

$$\lambda = k^2\rho^2\,,$$

ρ : gyration radius of the electron.

Now, we are interested in the resonant waves. The dispersion relation of such waves is derived from taking the limit $ck \to \infty$ or the refractive index $ck/\omega \to \infty$ in Eq. (3). The result is

$$\varepsilon_{zz} = 1 - \frac{2\omega_p^2}{\omega_b^2} \frac{e^{-\lambda}}{\lambda} \sum_{n=1}^{\infty} \frac{n^2 I_n(\lambda)}{(\frac{\omega}{\omega_b})^2 - n^2} = 0\,. \tag{6}$$

On the other hand, the dispersion relation derived by Bernstein, Eq. (46) of his paper [4], can be simplified, after some calculation, as follows:

$$k^2a^2 = 2e^{-\lambda} \sum_{n=1}^{\infty} \frac{n^2 I_n(\lambda)}{(\frac{\omega}{\omega_b})^2 - n^2}\,, \tag{7}$$

where a is the Debye length. Thus Eq. (6) is identical to Eq. (7) and the resonant waves of extraordinary ones are nothing but the longitudinal electron oscillations.

In the limit $\lambda = k^2\rho^2 \ll 1$, the case of gyration radius small compared with wavelength, Eq.(7) can be expanded into a series in λ as:

$$k^2a^2 = \sum_{n=1}^{\infty} \sum_{\ell=0}^{\infty} \sum_{m=0}^{\infty} (-1)^{\ell} \frac{\lambda^{n+\ell+2m}}{2^{n+2m-1}\,\ell!\,m!\,(n+m)!} \frac{n^2}{(\omega/\omega_b)^2 - n^2} , \tag{8}$$

or

$$\frac{\omega_b^2}{\omega_p^2} = \sum_{n=1}^{\infty} \sum_{\ell=0}^{\infty} \sum_{m=0}^{\infty} (-1)^{\ell} \frac{\lambda^{n+\ell+2m-1}}{2^{n+2m-1}\,\ell!\,m!\,(n+m)!} \frac{n^2}{(\omega/\omega_b)^2 - n^2} . \tag{9}$$

Equation (9) is an exact expression corresponding to Eq.(50) of Bernstein's paper. From Eq. (9) the magnetic field $(\omega_b/\omega)^2$ giving the resonant wave can be plotted against the electron density $(\omega_p/\omega)^2$ for the fixed frequency ω. Such a graph, denoted hereafter by $(\omega_b/\omega)^2 - (\omega_p/\omega)^2$ diagram, will be obtained from the following equation, which is deduced from Eq. (7),

$$\frac{1}{\eta} = \frac{2\gamma^2}{\varepsilon} \exp\left(-\frac{\varepsilon}{\gamma^2}\right) \sum_{n=1}^{\infty} \frac{n^2 I_n(\varepsilon/\gamma^2)}{1 - n^2\gamma^2} \tag{10}$$

Here

$$\eta = (\omega_p/\omega)^2 , \qquad \gamma = \omega_b/\omega ,$$

$$\varepsilon = (KT/m)k^2/\omega^2 , \qquad \lambda = k^2\rho^2 = \varepsilon/\gamma^2 .$$

The $\gamma^2 - \eta$ diagram can be calculated from Eq.(10), taking ε as a parameter. In our experiments, the temperature of plasma electrons T is low ($\sim 10^4$ °K) and k is the order of $2 \sim 10$ cm^{-1} ($2\pi/k$ being the order of diameter of plasma column), and also $\omega/2\pi \approx 9 \times 10^9$ cps, then $\varepsilon \approx 10^{-4}$. Therefore Eq.(9) is applicable even if harmonics up to the 30th are included, in which $\lambda \approx 10^{-1}$.

(i) For the $\gamma^2-\eta$ diagram in the interval $1>\gamma>\frac{1}{2}$ it is sufficient to keep the terms up to the 1st order with respect to λ in Eq. (9).
The result is

$$(\frac{\omega_b}{\omega_p})^2=\frac{1-\lambda}{\gamma^{-2}-1}+\frac{\lambda}{\gamma^{-2}-4} \tag{11}$$

or

$$\eta=\frac{(1-\gamma^2)(4\gamma^2-1)}{4\gamma^2-(1+3\varepsilon)} \tag{11'}$$

It is natural that, Eq. (11) reduces to the well-known equation,

$$\eta+\gamma^2=1 \qquad \text{or} \qquad \omega^2=\omega_p^2+\omega_b^2 \ ,$$

if the thermal motion of plasma electrons is neglected ($\varepsilon=0$). It is seen from Eq. (11)' that η becomes an infinity for

$$\gamma^2=\frac{1}{4}+\frac{3}{4}\varepsilon \equiv \gamma_2^2 \tag{13}$$

and η becomes zero for $\gamma^2=1-0$.
(ii) For the root in the interval $1>\gamma>\frac{1}{3}$ it is sufficient to keep the terms up to the 2nd order with respect to λ . Equation (9) yields

$$(\frac{\omega_b}{\omega_p})^2=\frac{1-\lambda+\frac{5}{8}\lambda^2}{\gamma^{-2}-1}+\frac{\lambda(1-\lambda)}{\gamma^{-2}-4}+\frac{\frac{3}{8}\lambda^2}{\gamma^{-2}-9} \tag{14}$$

or

$$\eta=\frac{(1-\gamma^2)(1-4\gamma^2)(1-9\gamma^2)}{(1+3\varepsilon+15\varepsilon^2)-(13+27\varepsilon)\gamma^2+36\gamma^4} \tag{14'}$$

Therefore, $\eta\to\infty$ for the following two values of γ^2 :

$$\left.\begin{aligned} \gamma^2 &= \frac{1}{4} + \frac{3}{4}\varepsilon - 3\varepsilon^2 \equiv \gamma_2^2 \ , \\ \gamma^2 &= \frac{1}{9} + 3\varepsilon^2 \equiv \gamma_3^2 \end{aligned}\right\} \tag{15}$$

and $\eta \to 0$ for $\gamma^2 \to 1-0$ and $\gamma^2 \to \frac{1}{4} - 0$.

(iii) Similarly, for the root in the interval $1 > \gamma > \frac{1}{4}$, keeping the terms up to the 3rd order, Eq. (7) yields

$$\begin{aligned} (\frac{\omega_b}{\omega_p})^2 = &\frac{1}{\gamma^{-2}-1}\{1-\lambda+\frac{5}{8}\lambda^2-\frac{1}{24}\lambda^3\} + \frac{\lambda}{\gamma^{-2}-4}(1-\lambda+\frac{7}{12}\lambda^2) \\ &+\frac{1}{\gamma^{-2}-9}\{\frac{3}{8}\lambda^2(1-\lambda)\} + \frac{1}{\gamma^{-2}-16}(\frac{\lambda^3}{12}) \end{aligned} \tag{16}$$

or

$$\eta = \frac{(1-\gamma^2)(1-4\gamma^2)(1-9\gamma^2)(1-16\gamma^2)}{(1+3\varepsilon+15\varepsilon^2+105\varepsilon^3)-(29+75\varepsilon+240\varepsilon^2)\gamma^2+(244+432\varepsilon)\gamma^4-576\gamma^6} \tag{16'}$$

Therefore, $\eta \to \infty$ for the following values of γ^2 :

$$\left.\begin{aligned} \gamma^2 &= \frac{1}{4} + \frac{3}{4}\varepsilon - 3\varepsilon^2 + 23.2\varepsilon^3 \equiv \gamma_2^2 \ , \\ \gamma^2 &= \frac{1}{9} + 3\varepsilon^2 - 43.2\varepsilon^3 \equiv \gamma_3^2 \ , \\ \gamma^2 &= \frac{1}{16} + 20\varepsilon^3 \equiv \gamma_4^2 \ , \end{aligned}\right\} \tag{17}$$

and $\eta \to 0$ for $\gamma^2 \to 1-0$, $\frac{1}{4}-0$ and $\frac{1}{9}-0$.

Clearly the similar results can be obtained for other branches of the higher order more than the 4th ($\gamma < \frac{1}{4}$), although the calculation becomes more complicated.

In Figs. 1 and 2 are plotted $(\omega_b/\omega)^2-(\omega_p/\omega)^2$ and $(\omega_b/\omega)-(\omega_p/\omega)^2$ diagrams respectively, computing numerically on Eqs. (11)', (14)' and (16)' with ε as a parameter. It is seen that these curves approach asymptotically to the curves of $\omega^2 = \omega_p^2 + \omega_b^2$ and of the cyclotron harmonics $\omega = n\omega_b$

when ε becomes more and more small.

The gaps in the spectrum of possible frequencies in the vicinity of the cyclotron harmonics, described by Bernstein, can be replaced by the gaps of the magnetic field in our treatments. The widths of these gaps, which correspond to those of the magnetic fields where the rf waves cannot propagate, can readily be calculated from Eq. (17). At the 2nd, 3rd and 4th harmonics, these widths are given by:

$$\begin{aligned} \Delta \gamma_2^2 &= \gamma_2^2 - \frac{1}{4} \approx \frac{3}{4}\varepsilon , \\ \Delta \gamma_3^2 &= \gamma_3^2 - \frac{1}{9} \approx 3\varepsilon^2 , \\ \Delta \gamma_4^2 &= \gamma_4^2 - \frac{1}{16} \approx 20\varepsilon^3 , \end{aligned} \tag{18}$$

The corresponding width of the magnetic field strength at the 2nd harmonics is

$$\Delta\gamma_2 = \frac{\Delta\omega_{b2}}{\omega} \approx \frac{1}{2}\frac{1}{(\gamma)_{\gamma=3/2}}\Delta\gamma_2^2 = \frac{3}{4}\varepsilon = \frac{3}{4}\frac{KT}{m}\frac{k^2}{\omega^2} \tag{19}$$

or

$$\Delta B_2 = \frac{3}{4}\frac{m}{e}\left(\frac{KT}{m}\right)\left(\frac{k}{\omega}\right)^2\omega . \tag{19'}$$

Similarly, at tht 3rd harmonics

$$\frac{\Delta\omega_{b3}}{\omega} \approx \frac{9}{2}\varepsilon^2 = \frac{9}{2}\left(\frac{KT}{m}\right)^2\left(\frac{k}{\omega}\right)^4 \tag{20}$$

or

$$\Delta B_3 \approx \frac{9}{2}\frac{m}{e}\left(\frac{KT}{m}\right)^2\left(\frac{k}{\omega}\right)^4\omega . \tag{20'}$$

And at the 4th harmonics

$$\frac{\Delta\omega_{b4}}{\omega} \approx 40\,\varepsilon^3 = 40\,(\frac{KT}{m})^3\,(\frac{k}{\omega})^6 \qquad (21)$$

or

$$\Delta B_4 \approx 40\,\frac{m}{e}\,(\frac{KT}{m})^3\,(\frac{k}{\omega})^6\,\omega\,. \qquad (21')$$

It is seen from the above equations that the widths of these gaps become small with decreasing the electron temperature and with increasing the number of cyclotron harmonics.

In our experimental conditions, $\varepsilon \approx 10^{-4}$ and. $\omega/2\pi \approx 10$ Gc, these widths are $\Delta B_2 \approx 0.25$, $\Delta B_3 \approx 2\times10^{-5}$ and $\Delta B_4 \approx 2\times10^{-7}$ (gauss). Therefore, considering from the experimental standpoints, it is the same as saying that there are no gaps in our case.

§ 3 Experimental Apparatus and Procedures

The discharge tube used is 13mm in inner diameter as shown in Fig.3. An anode was a tantalum cylinder of 10 mm in diameter and 20 mm in length with one end plate and set 900 mm away from a cathode. The indirectly heated oxide cathode consisted of the two coaxial hollow cylinder with four spacing walls, 10 mm in outer diameter and 33 mm in length. This tube was inserted into the holes of pieces of the electromagnet and was in part within a waveguide running perpendicular to it as shown in Fig. 3. This waveguide was square and had a side equal to the longer side of the standard X-band guides, which were connected through the tapered parts to it.

The intensity of the magnetic field between these two conically shaped pieces with holes of 16 mm in diameter and apart 80 mm from each other was measured by a gauss-meter. In Fig. 3 are plotted the intensity distributions of the field along a axial as well as a radial direction. It is seen from Fig. 3 that the magnetic field is homogeneous within 2 % over the positive column in a waveguide, the microwave radiation from

which was measured. At the same time, the field intensity at the centre was measured by a protron-meter as a function of field coil current. The magnetic field was impressed on a part of positive column, which was $\sim$ 10 % of the total length of positive column, and parallel to the direction of discharge current.

The positive column between the pole pieces became more slender with increasing the intensity of a magnetic field at rather low gas pressure. For example, at the pressure of 10 mmHg, the positive column in the magnetic field was seen inside the tube all over, but at the pressure of 10^{-2} mmHg and above the magnetic field intensity of about one thousand gausses, the diameter of column became several mm and at the small discharge current a plasma of that portion was disappeared in the anode side.

The measurements of microwave radiation from a plasma were performed by means of X-band radiometer. The axis of its square waveguide was perpendicular to the magnetic field $\vec{B}$ and the rf electric vector in the guide was also perpendicular to $\vec{B}$. Therefore, the extraordinary and plasma waves, propagating transversely to $\vec{B}$, might be detected. The radiometer used in this work was operated at the fixed frequency, $\omega/2\pi = 9,485$ Mc with a 5 Mc band width, the image of a heterodyne detection being cut.

When the magnetic field was swept at a constant discharge current I_d and the radiometer output was continuously traced on the recorder, the radiation pattern, denoted hereafter by $P(I_d)-B$ patterns, was displayed, in which x- and y- axis were proportional to the magnetic field strength B and to the radiated power respectively. In the same way, $P(B=0)-I_d$ pattern was recorded by varying the discharge current I_d, being fed into x-axis at no magnetic field. In the figure illustrating the radiation patterns, the zero level of radiation power from plasma was set at the noise power of radiometer itself, and each pattern was displaced relatively to each other on y-axis and also the scale of x-axis was normalized to

the cyclotron field $B_c = (m/e)\omega = 3,387$ gausses, that is, plotted in ω_b/ω.

§ 4 Experimental Results and Discussions

In Fig. 4 are shown a series of the radiation patterns ($P(I_d)$-B) on a weakly ionized, high-pressure discharge in neon. At small currents ($I_d \lesssim 5$mA) or low electron densities $\omega_p/\omega \ll 1$, there appears the resonant peak at the cyclotron field $\omega_b/\omega = 1$. As the current increases ($I_d \approx 5-50$mA) this peak becomes large in intensity and shifts to a lower magnetic field ($\omega_b/\omega < 1$). When the current increases further, however, the peak becomes small and broad in appearance, because the radiated power at $B = 0$ becomes large. Although the peak cannot be identified clearly at these large I_d, the peak seems to shift gradually to a low magnetic field with increasing I_d and disappear near the $\omega_b/\omega = 0$, when the radiation power at zero field reaches the blackbody. It is to be noted that the faint resonant peaks superimposed on a background radiation are observed in the neighbourhood of the 2nd harmonics of the cyclotron field $\omega_b/\omega = \frac{1}{2}$ for some large I_d ($I_d \gtrsim 0.9$A).

The radiation patterns on a intermediate-pressure discharge in argon exhibit the resonant peaks near the 2nd, 3rd, 4th and 5th cyclotron harmonics at a large discharge current, in addition to the main peak, as shown in Fig. 5. The similar radiation patterns are measured on the discharges in krypton and xenon (Figs.6 and 7). The amplitude of a given harmonics (for example, see the 2nd harmonics of Fig. 6) increases with the discharge current and also these peaks seem to dip below the background radiation on the small side of the magnetic field relative to the harmonics as reported by Bekefi et al.[11]. Furthermore, these anomalous resonant peaks are also observed by measuring the transmission and reflection from these plasmas. Strictly speaking, the radiation patterns illustrated in this paper must be corrected by taking account of

the reflection from the plasma. It was shown from the experiments, however, that this effect was rather small and the radiation patterns were not altered substantially.

In order to compare the experimental results with the theoretical, the field strength giving the resonant peak on the radiation pattern illustrated in Fig. 4 is plotted against the discharge current I_d. $A(\omega_b/\omega) - I_d$ diagram obtained by such a way is shown in Fig. 10 , which represents a relation between the magnetic field (ω_b/ω) and the discharge current I_d for the resonant radiation detected with the fixed frequency ω. (The short vertical hars in this figure represent the broad and faint peaks in radiation patterns.) It is found from this figure that the experimental plots seem to be divided into the two branches, each branch approarching asymptotically to the line of the 2nd harmonics $\omega_b/\omega = \frac{1}{2}$ and to the dotted curve. Since it has been observed that the plasma type resonant radiation ocurrs at $\omega^2 = \omega_p^2 + \omega_b^2$, the dotted curve, which depends on the discharge current I_d or plasma frequency as well as the magnetic field (ω_b/ω) , is possibly interpreted as the P-type curve given by Eq. (1). Accordingly, the experimental plots may be considerd to correspond to the theoretical curve given in Fig. 2, with the exception that the former takes I_d , while the latter $(\omega_p/\omega)^2$ as an abscissa. The apparent difference of P-type curve between Figs. 2 and 10 can be explained as follows: Since the contraction of plasma column ocurrs gradually with increasing a magnetic field up to, say, 1 kilogauss ($\omega_b/\omega \approx 1/3$) , the P-type curve of (ω_b/ω) - I_d diagram is enlarged along abscissa whithin $\omega_b/\omega \lesssim 1/3$, compared with that of (ω_b/ω) - (ω_p/ω)^2 diagram.

The radiation patterns on a relatively low pressure discharge are shown in Fig. 8 and (ω_b/ω) - I_d diagrams in Figs. 11 and 12. Since the P-type radiations no longer can be traced clearly in the range of $\omega_b/\omega \lesssim \frac{1}{2}$ from the complicated radiation patterns as shown in Fig. 8,

the P-type curves (the dotted) are drawn appropriately for reference in Figs.10~13, by measuring the P-type curve in the range, $1 > (\omega_b/\omega) > \frac{1}{2}$, and the discharge current at which the radiation with no magnetic field reaches the blackbody. Since the peaks at the 2nd harmonics seem to dip below the background radiation and then increase rapidly with increasing the magnetic field as shown in Fig. 8, the field intensity at which these peaks increase steeply is plotted by the short transverse bars in $(\omega_b/\omega) - I_d$ diagram. The other weak resonant peaks are observed on the left side of P-type radiations within small discharge current as seen in Fig.8, but these are not understood as yet. The experimental plots in $(\omega_b/\omega) - I_d$ diagram (see Figs. 11 and 12) have four branches, which seem to correspond to the theoretical in Fig. 2. The number of these branches increases with decreasing the gas pressure, as shown in Fig. 13. The corresponding radiation patterns are shown in Fig. 9, in which the successive harmonics as many as 9th harmonics can be observed.

In the region denoted by X in $(\omega_b/\omega) - I_d$ diagram (Fig.13) the peculiar peaks are observed in the vicinity of the 2nd harmonics. As shown in Fig. 14, several peaks at $\omega_b/\omega \approx \frac{1}{2}$ are seen on the $P(I_d) - B$ patterns in the current range of $I_d \approx 50 \sim 120$ mA, and at more large current, they disappear and the radiation merely increases steeply at the 2nd harmonics. It is understood from $(\omega_b/\omega) - I_d$ diagram (Fig. 15) obtained from Fig. 14 that such peaks constitute several series and each of which becomes appeared at slightly larger magnetic field than the 2nd harmonics and disappeared at the 2nd harmonics, the magnitude of which being maximum at the 2nd harmonics. The physical mechanism for this fine structure at the 2nd harmonics spectrum is not understood as yet, though the propagation of surface wave on the magnetoplasma or the standing wave in the plasma column is considered. Recently such peculiar peaks are observed also by Kojima et al.[16].

Now it may be reasonable to consider from the above mentioned experi-

mental results that the plasma type radiation detected has the harmonic structure: The experimental curve in $(\omega_b/\omega) - I_d$ diagram (Figs.10~13) can be composed of the several branches, each of which approaches asymptotically to the curves of $\omega^2 = \omega_p^2 + \omega_b^2$ and of the cyclotron harmonics $\omega = n\omega_b$. Thus the experimental curve corresponds to the theoretical one plotted in Fig. 2. The gaps in the spectrum of allowed frequencies at cyclotron harmonics could not be measured, since these gaps in the magentic field in our experiments are very small as calculated in § 2 and the peaks at harmonics are rather broad, compared with the theoretical values of gaps. The amplitudes of the successive harmonics, although they are decreasing, are of the same order of magnitude and their widths decrease slightly with increasing the harmonics number, and the peak disappears into the background radiation near the highest harmonics observed. Furthermore, the number of the successive harmonics increases with the discharge current, untill it saturates above some discharge current, its saturated value of the highest harmonics number being denoted by N_{max}. The cyclotron harmonics are observed independently of the kind of gas used and N_{max} increases with decreasing the gas pressure as shown in Figs. 16~19. Comparing at the same gas pressure, N_{max} decreases in the order of Ne, Ar, Kr and Xe plasmas and especially N_{max} for Ne is much larger than those for other three gases, whose N_{max}'s are almost equal. These circumstances just correspond to the collision frequency between the electron and the nutral particles ν_{en} and it may be inferred that N_{max} increases with decreasing ν_{en}. Although the line shapes of the harmonics cannot be determined exactly, being superimposed on the background radiation, it seems that their peaks are rather asymmetrical and their widths do not depend on the gas pressure and also these peaks have a tendency to occur at slightly larger magnetic field than the harmonics field.

The radiations at the cyclotron harmonics was investigated theoretic-

ally by Sugihara[17] recently and he found that when a charge moves along a magnetic field with a fast but non-relativistic velocity, the discrete peaks appear in the spectrum of radiation near the cyclotron harmonics. This theory may be a possible explanation of the origin of cyclotron harmonics described above.

It is to be noted that the resonant peaks at the succesive harmonics were detected also for the ordinary wave propagating perpendicular to a magnetic field [18].

The extensive effort was made to detect the intense radiation due to the negative absorption effect at the cyclotron resonance in slightly ionized gases. Such radiations were observed in Xe, Kr, and Ar plasmas alone when the whole discharged tube inclusive of cathode was placed in a longitudinal magnetic field as reported[14]. But these radiations were never observed on any pressure range of Xe, Kr, and Ar gases in this work, where a part of the positive column was immersed in the magnetic field as shown in Fig. 3.

§ 5 Conclusion

The resonant radiation from a magnetoactive plasma for the extra-ordinary wave, propagating perpendicular to a magnetic field was investigated. Applying the theoretical results made by Bernstein to our experimental condition, it was shown that the plasma type radiation has the harmonic structure: When the thermal motion of plasma electron is considered, the curve of P-type radiation given by Eq. (1) is divided into many branches, each of which approaches asymptotically to the curves of Eq. (1) and of the cyclotron harmonics $\omega = n\omega_b$ as shown in Figs. 1 and 2.

The microwave radiations from the magnetoactive plasmas in a waveguide were measured and the characteristic of their resonant radiations was investigated. Their experimental plots in $(\omega_b/\omega) - I_d$ diagram, where the field strength of the resonant radiations being plotted against the dis-

charge current, were considered to correspond to the theoretical curve shown in Fig. 2. Thus these observed radiations were interpreted as the plasma type ones, their dispersion relation having the harmonic structure. The gaps in the spectrum at cyclotron harmonics were not observed, because these gaps were considered to be within the experimental error in our experimental conditions.

The maximum number of the successive harmonics increased with decreasing the gas pressure, independently of the kind of gas. Since the line shape of the cyclotron harmonics was not determined experimentally, the detailed study for theses was not made as yet. At the low pressure discharge the fine structure of resonant peaks was observed in the vicinity of the 2nd harmonics, no physical meaning for these phenomena being known.

Acknowledgement

The suthors wish to express their sincere thanks to Professor I. Takahashi, Kyoto University, for his guidance and encouragement, and also to Professor K. Takayama and Dr. H. Ikegami for their interests and valuable discussions. The authors are grateful to Dr. M. Imai, Manager of the Research Laboratory, Kawasaki Steal Corporation for providing the electromagnet and to Dr. Y. Ishikawa, Manager of the Research Laboratory, Nippon Electric Co., for preparing the discharge tubes. Their thanks are also due to Mr. Y. Terumichi and Mr. M. Doi for help in the experiments. This research was partly supported by a research grant of the Ministry of Education.

References

1) V.L. Ginzburg: Propagation of Electromagnetic Waves in Plasma (North-Holland Publishing Co., Amsterdam, 1961).

2) E. P. Gross: Phys. Rev. 82 (1951) 232.

3) A.G. Sitenko et al.: Soviet Physics JETP 4 (1957) 512.

4) I.B. Bernstein : Phys. Rev. 109 (1958) 10.

5) S.C. Brown et al.: Phys. Rev. 122 (1961) 719.

6) S. Miyoshi: J. Phys. Soc. Japan 17 (1962) 1206.

7) K. Mitani and H. Kubo: J. Phys. Soc. Japan 16 (1961) 1480, Kakuyugo-Kenkyu 6 (1961) 417. (in Japanese)

8) S. Tanaka: Memoirs of the College of Science, University of Kyoto, Series A, 29 (1961) 361, 371, 381.

9) K. Kato: J. Phys. Soc. Japan 15 (1960) 1093.

10) G. Landauer: Proceeding of 5th International Conf. on Ionization Phenomena in Gases, Munich, 1961 (North-Holland Publishing Co., Amsterdam 1962).

11) G. Bekefi et al: Phys. Rev. Letters 9 (1962) 6.

12) K. Mitani, H. Kubo and S. Tanaka: Kakuyugo-Kenkyu 9 (1962) 267. (in Japanese)

13) H. Kubo, S. Tanaka and K. Mitani: Kakuyugo-Kenkyu 9 (1962) 188. (in Japanese)

14) S. Tanaka, K. Mitani and H. Kubo: Kakuyugo-Kenkyu 9 (1962) 473. (in Japanese) IPPJ-6 (Feb. 1963)

15) Y. N. Dnestrovskii and D. P. Kostomarov: Soviet Physics JETP 14 (1962) 1089.

16) S. Kojima et al: (private communication).

17) R. Sugihara: J.Phys. Soc. Japan 18 (1963) 1062.

18) H. Kubo, S. Tanaka and K. Mitani: Kakuyugo-Kenkyu 11 (1963) 58. (in Japanese)

List of Figure Captions

Fig. 1 $(\omega_b/\omega)^2 - (\omega_p/\omega)^2$ diagram

Fig. 2 $(\omega_b/\omega) - (\omega_p/\omega)^2$ diagram

Fig. 3 Magnet and discharge tube assembly

Fig. 4 Radiation patterns on Ne(p=7.8mmHg)

Fig. 5 Radiation patterns on Ar($p=8.0\times10^{-1}$)

Fig. 6 Radiation patterns on Kr($p=9.5\times10^{-1}$)

Fig. 7 Radiation patterns on Xe(p=1.05)

Fig. 8 Radiation patterns on Ar($p=1.5\times10^{-2}$)

Fig. 9 Radiation patterns on Ne($p=1.25\times10^{-1}$)

Fig. 10 $(\omega_b/\omega) - I_d$ diagram on Ar (p=3.1)

Fig. 11 $(\omega_b/\omega) - I_d$ diagram on Ar ($p=5.4\times10^{-2}$)

Fig. 12 $(\omega_b/\omega) - I_d$ diagram on Ar ($p=1.5\times10^{-2}$)

Fig. 13 $(\omega_b/\omega) - I_d$ diagram on Ne ($p=1.25\times10^{-1}$)

Fig. 14 Radiation patterns on Ne ($p=6\times10^{-2}$)

Fig. 15 $(\omega_b/\omega) - I_d$ diagram on Ne ($p=6\times10^{-2}$)

Fig. 16 N_{max} - pressure on Ne

Fig. 17 N_{max} - pressure on Ar

Fig. 18 N_{max} - pressure on Kr

Fig. 19 N_{max} - pressure on Xe

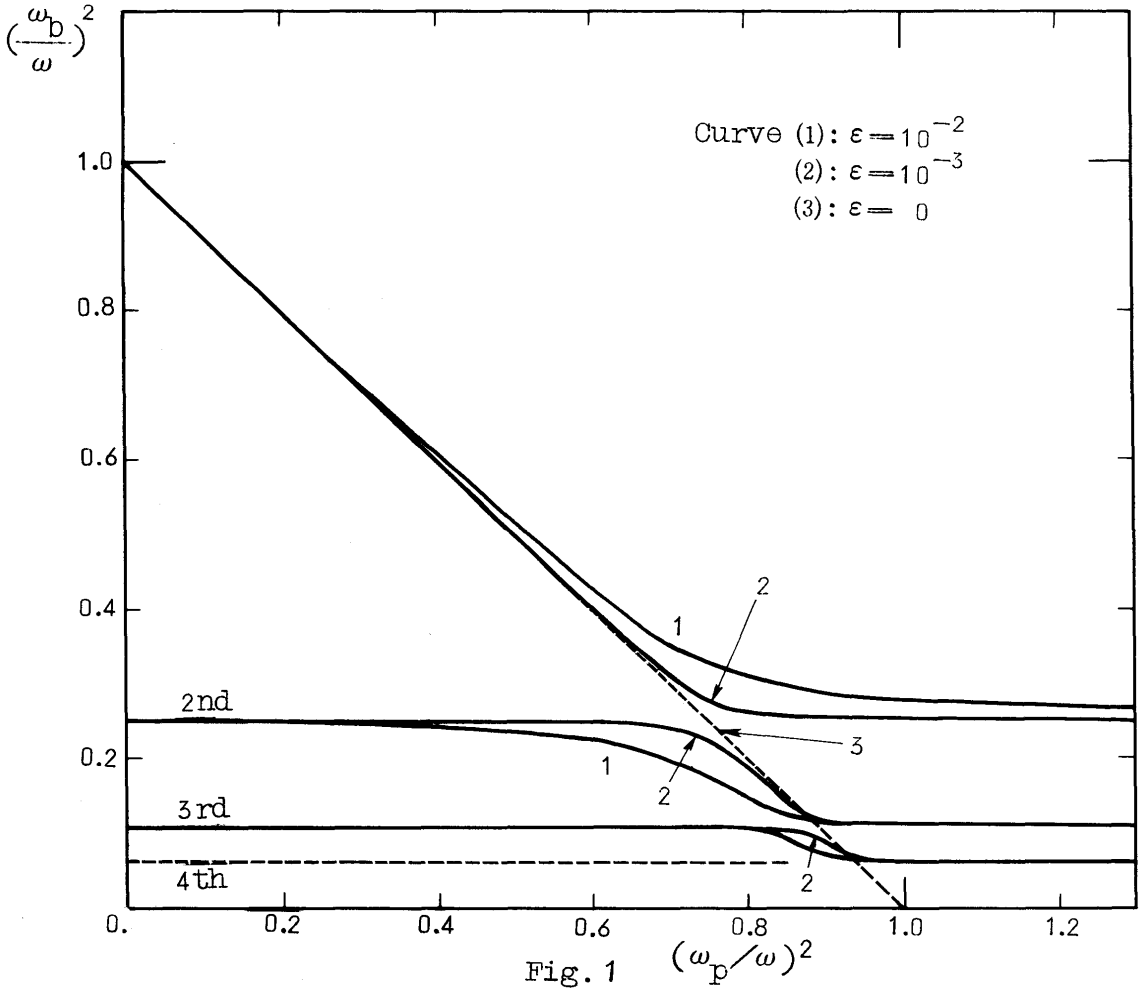
$(\frac{\omega_b}{\omega})^2$
Curve (1): $\varepsilon = 10^{-2}$
(2): $\varepsilon = 10^{-3}$
(3): $\varepsilon = 0$
1.0
0.8
0.6
0.4
0.2
0.
0.2
0.4
0.6
0.8
1.0
1.2
2nd
3rd
4th
1
2
3
$(\omega_p/\omega)^2$

Fig. 1

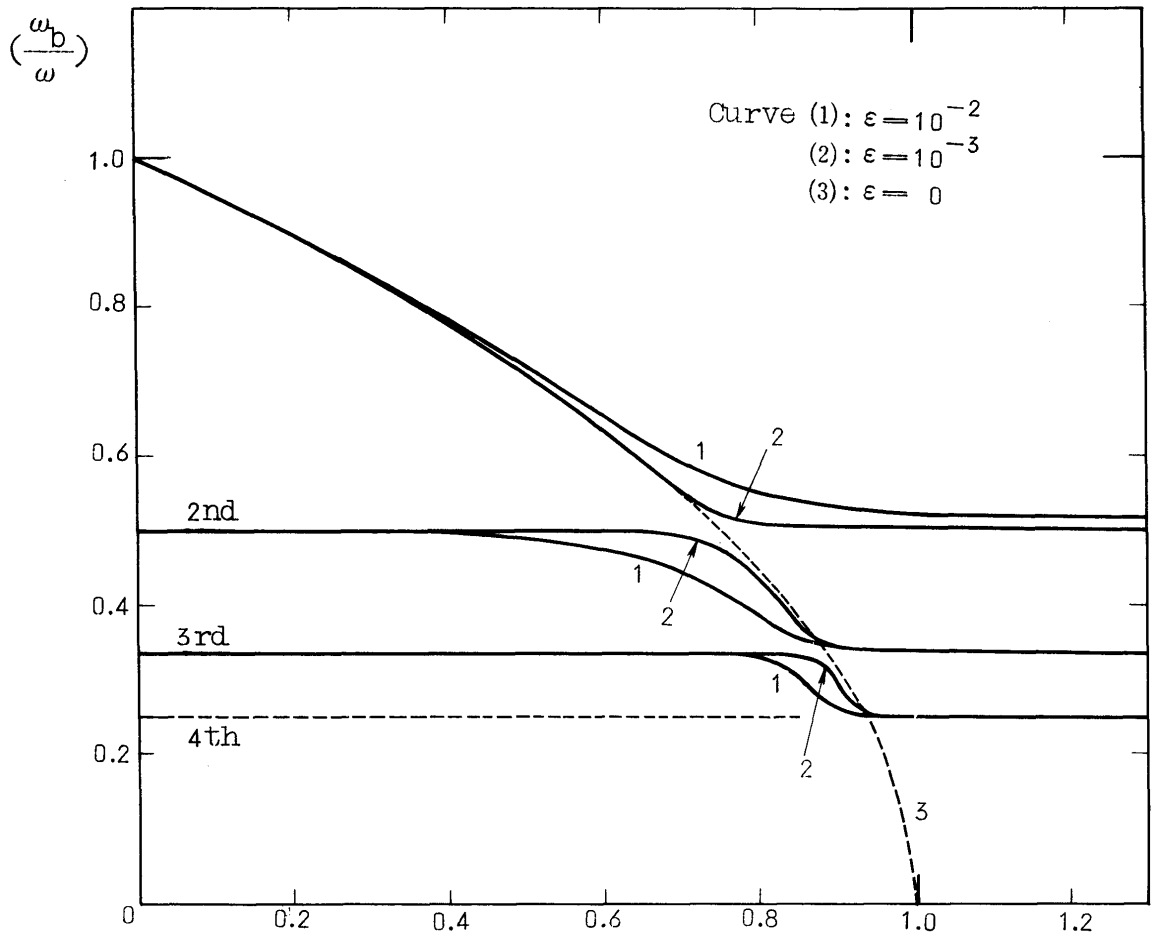

Fig. 2 $(\omega_p/\omega)^2$

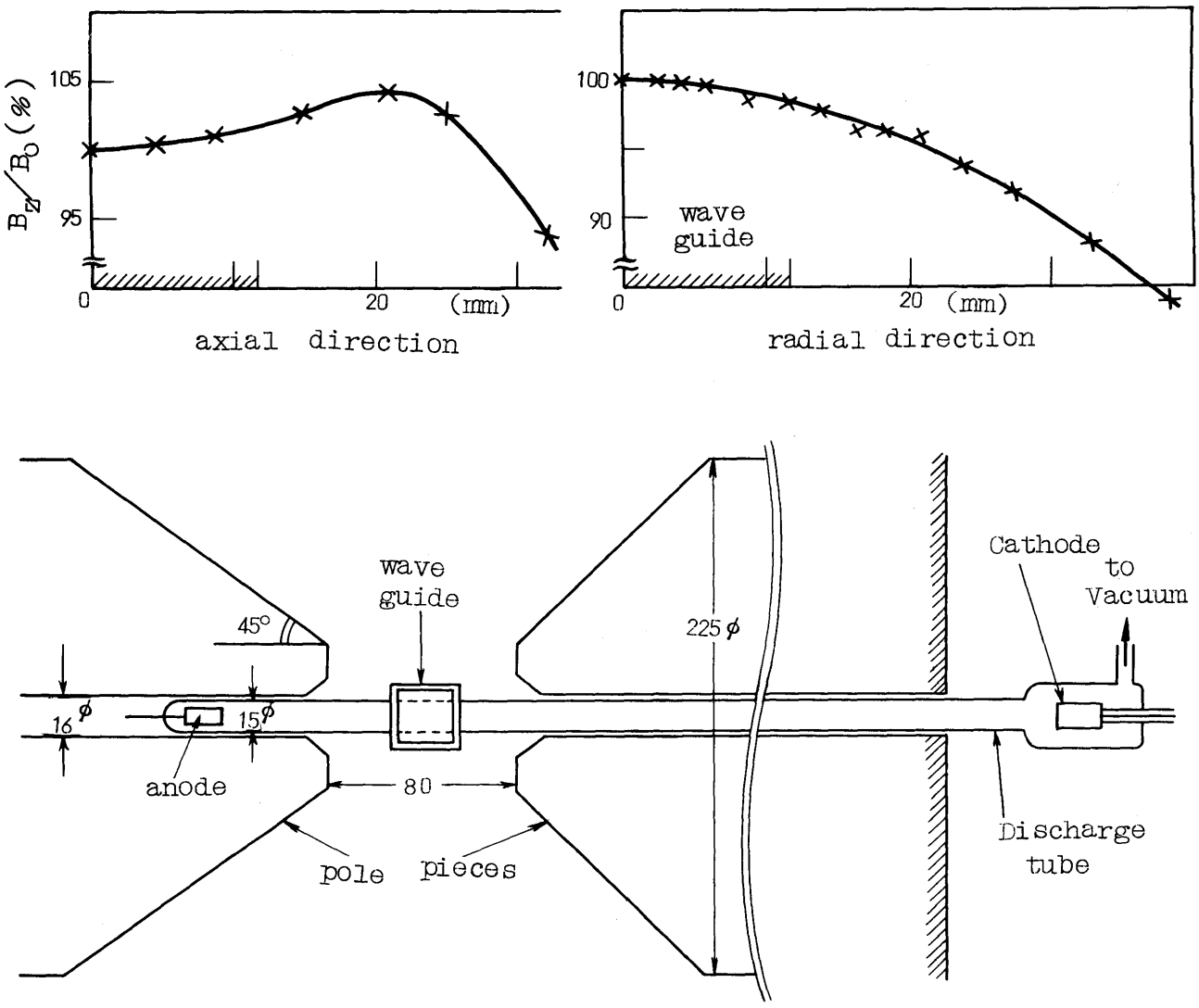
105
95
B_z/B_0 (%)
0
20 (mm)
axial direction
100
90
wave guide
0
20 (mm)
radial direction
wave guide
45°
16 φ
15 φ
anode
80
pole pieces
225 φ
Cathode
to Vacuum
Discharge tube

Fig. 3

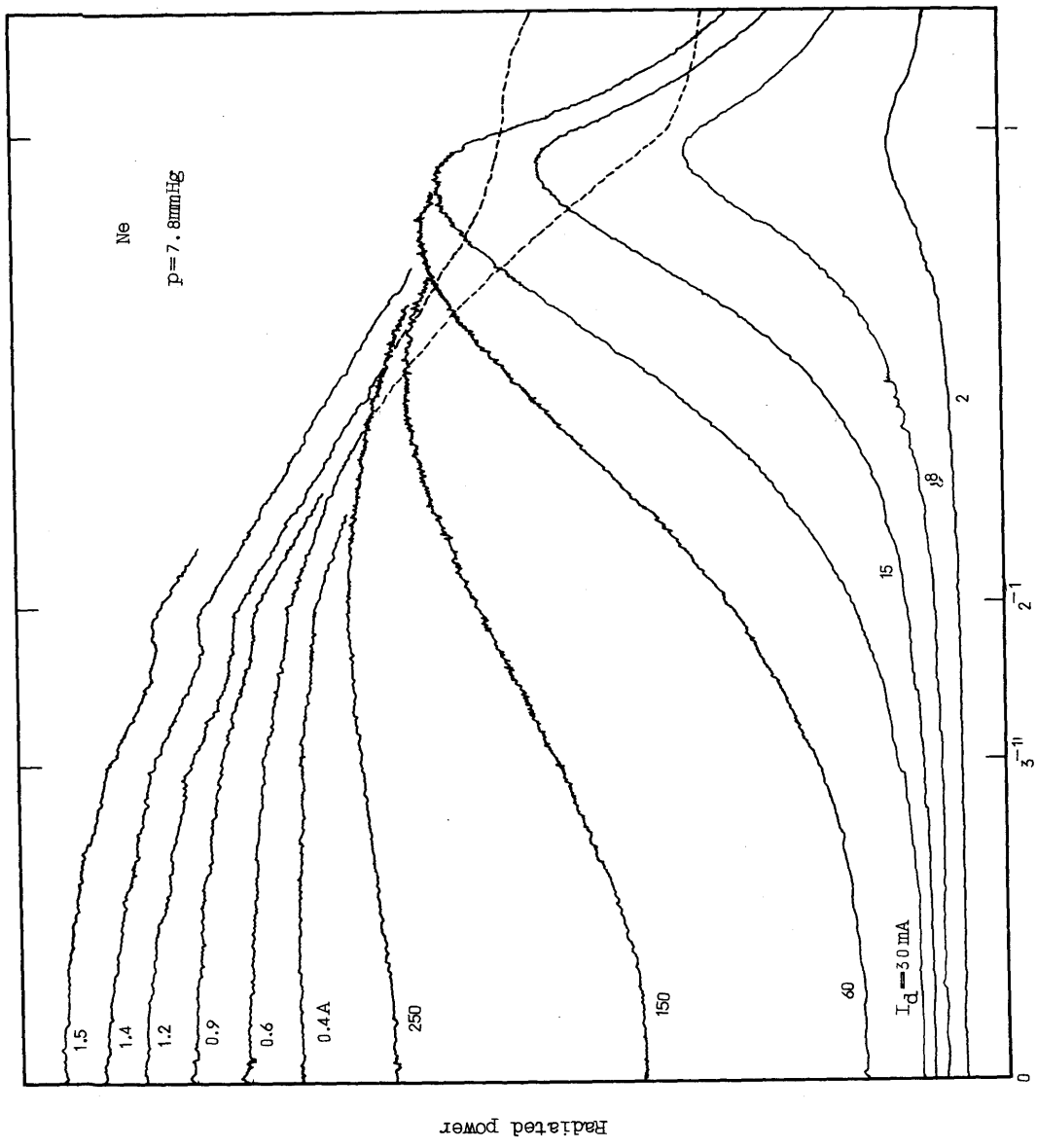
Ne
p=7.8mmHg
1.5
1.4
1.2
0.9
0.6
0.4A
250
150
60
15
8
2
I_d=30mA
0
2^{-1}
3^{-11}
1
Radiated power
Magnetic field (ω_b/ω)

Fig. 4

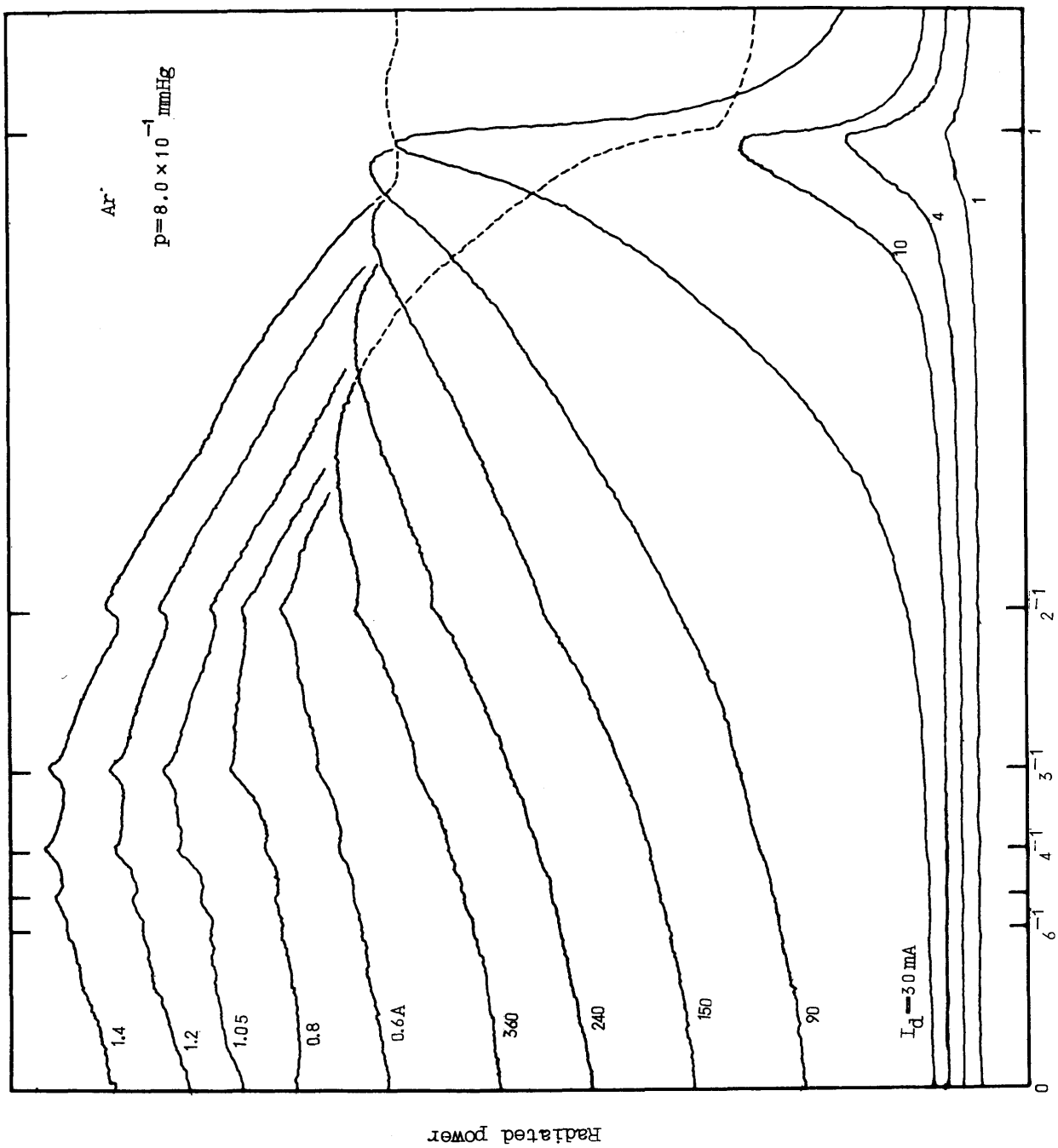
Ar
p=8.0×10⁻¹ mmHg
1.4
1.2
1.05
0.8
0.6A
360
240
150
90
I_d=30 mA
10
4
1
0
6^{-1}
4^{-1}
3^{-1}
2^{-1}
1
Radiated power
Magnetic field (ω_D/ω)

Fig.5

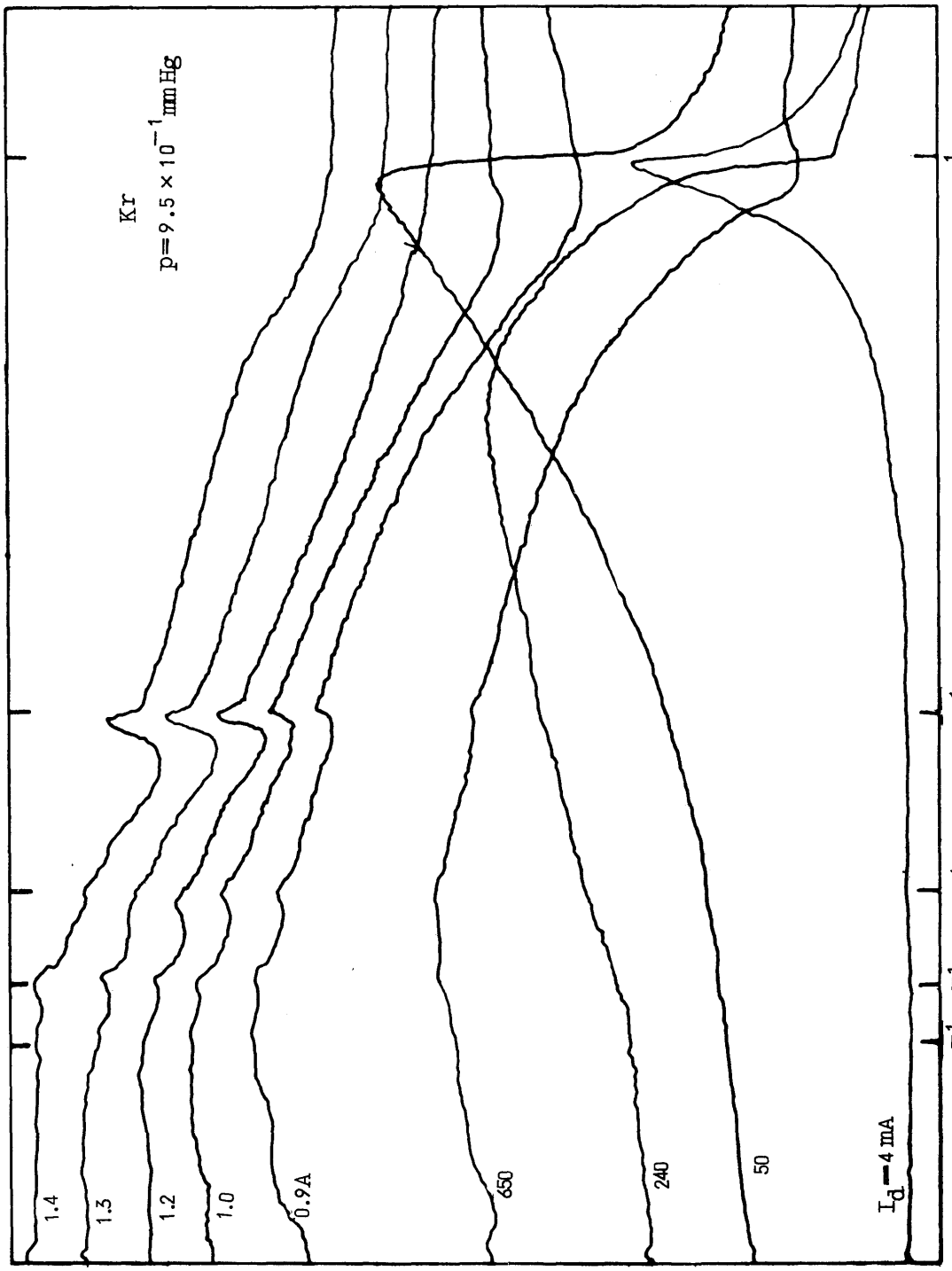
Kr
p=9.5 × 10⁻¹ mmHg
1.4
1.3
1.2
1.0
0.9A
650
240
50
Id=4 mA
1
2⁻¹
3⁻¹
4⁻¹
5⁻¹
Radiated power
Magnetic field (ω0/ω)

Fig. 6

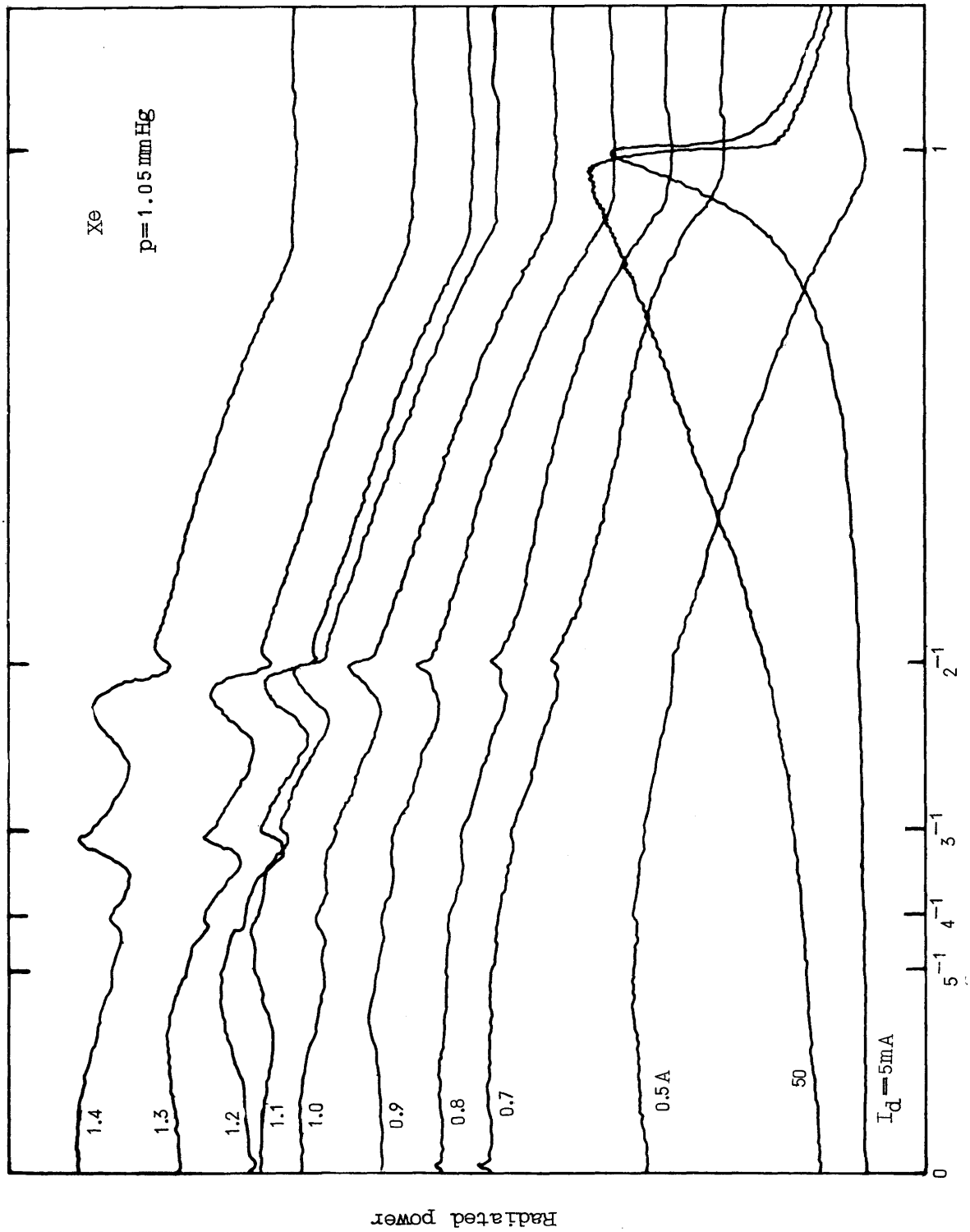
Xe
p=1.05 mm Hg
1.4
1.3
1.2
1.1
1.0
0.9
0.8
0.7
0.5A
50
I_d=5mA
0
5^{-1}
4^{-1}
3^{-1}
2^{-1}
1
Radiated power

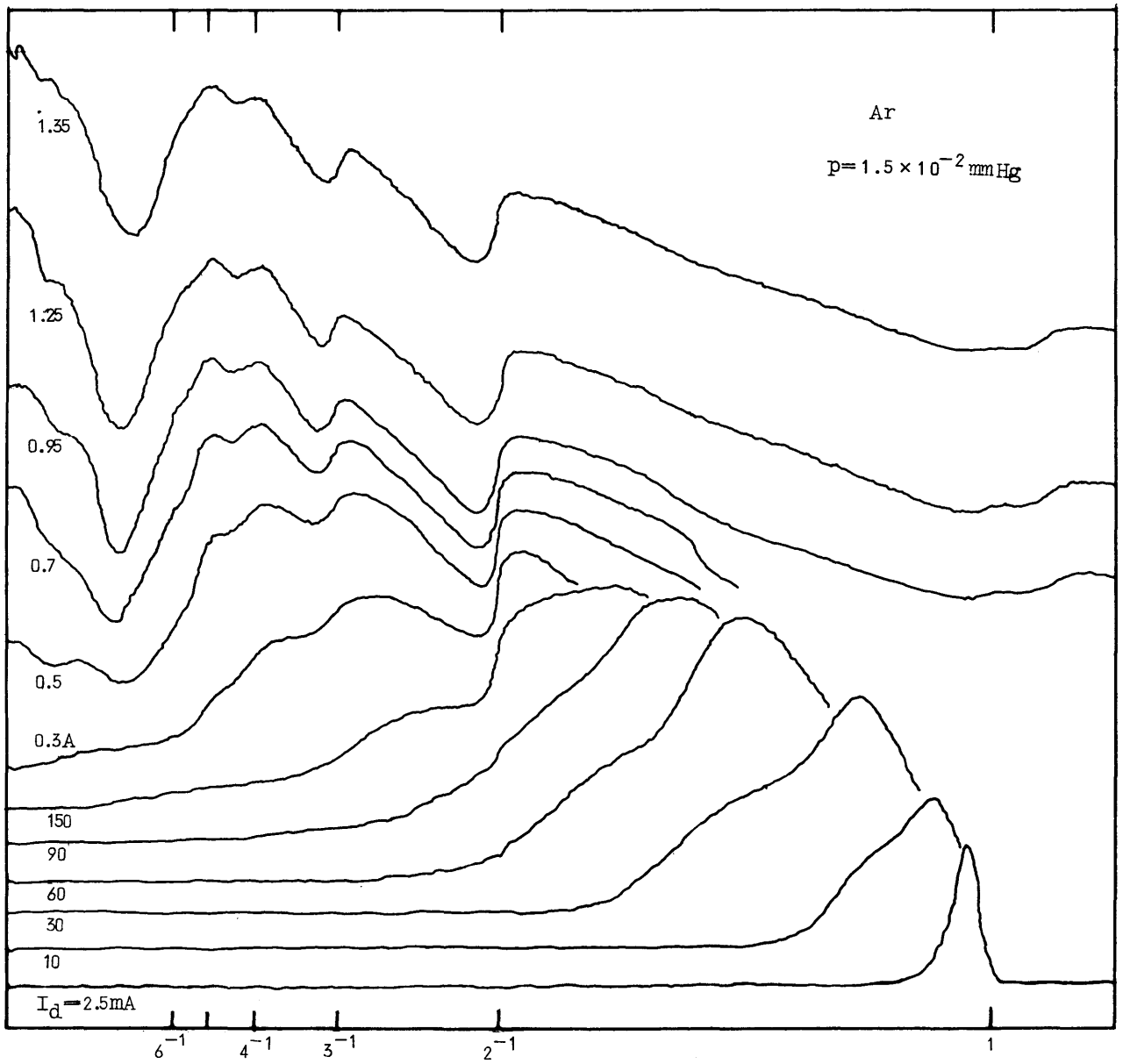
Ar
p=1.5×10⁻² mmHg
1.35
1.25
0.95
0.7
0.5
0.3A
150
90
60
30
10
Id=2.5mA
Radiated power
6⁻¹
4⁻¹
3⁻¹
2⁻¹
1
Magnetic field (ωb/ω)

Fig. 8

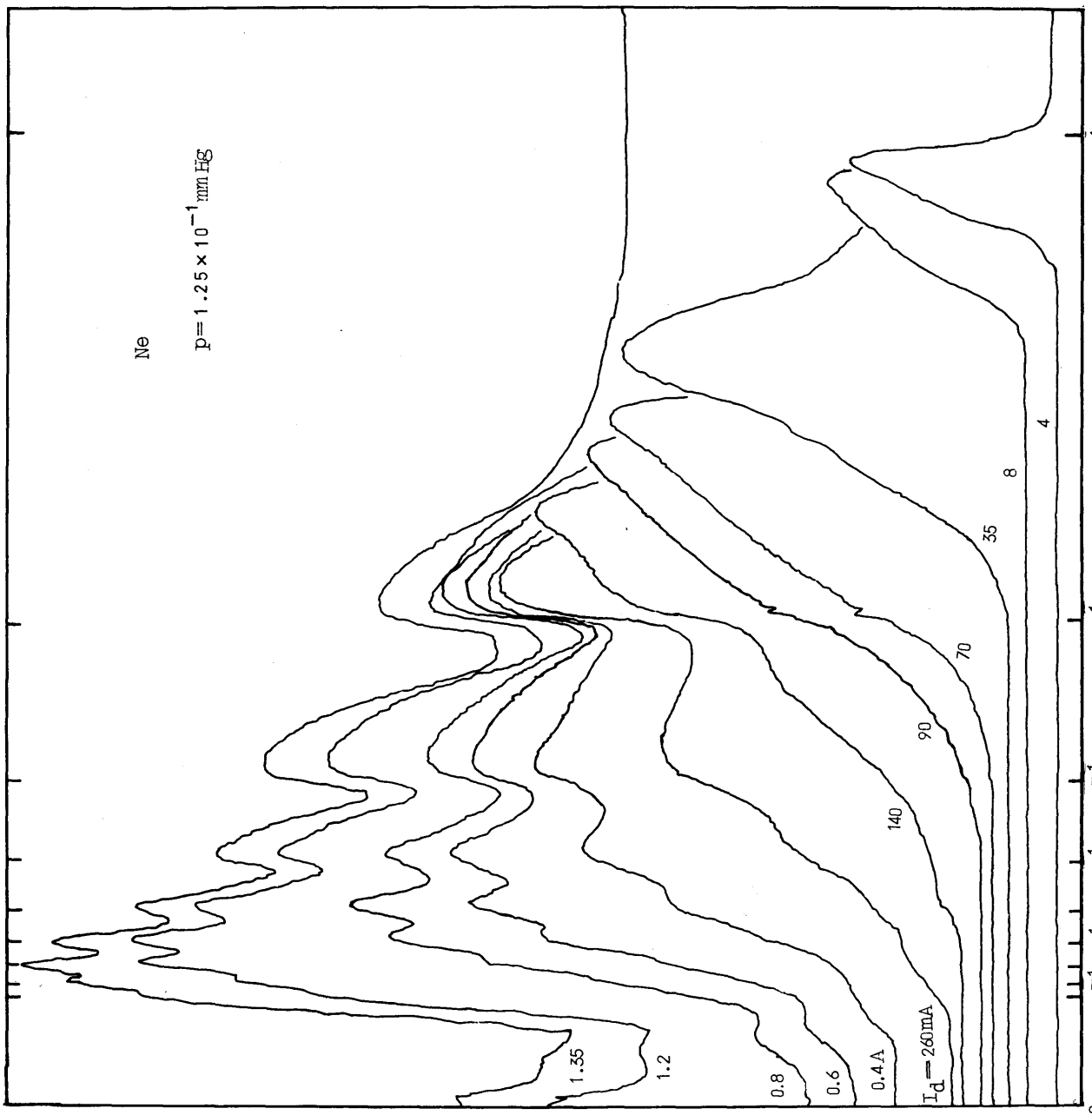
Ne
p= 1.25 × 10⁻¹ mm Hg
Id = 260mA
0.4A
0.6
0.8
1.2
1.35
140
90
70
35
8
4
0
8⁻¹
6⁻¹
4⁻¹
3⁻¹
2⁻¹
1
Radiated power
Megnetic field (ωb/ω)

Fig. 9

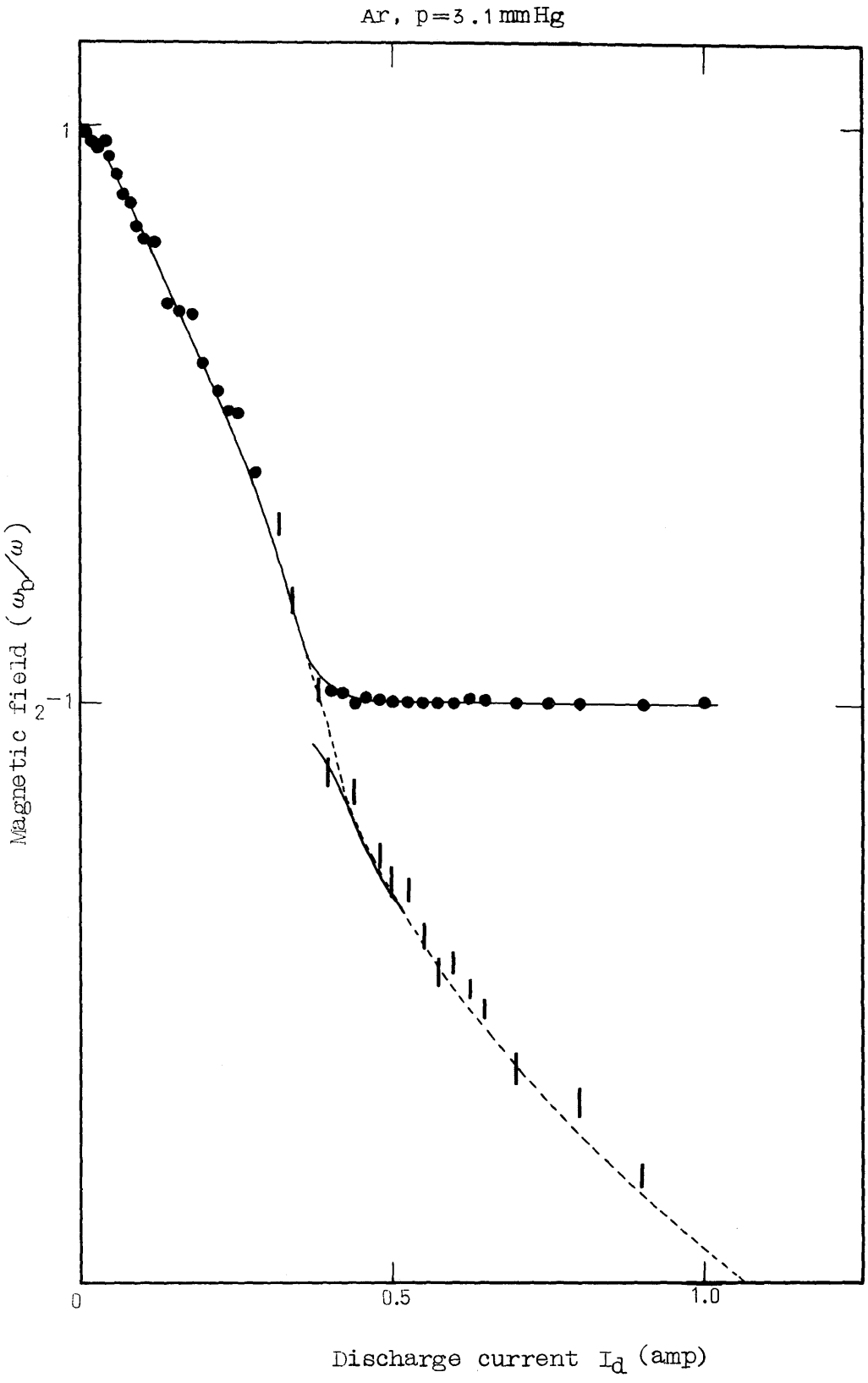
Ar, p=3.1 mmHg
1
2
1
Magnetic field (ω_b/ω)
0
0.5
1.0
Discharge current I_d (amp)

Fig. 10

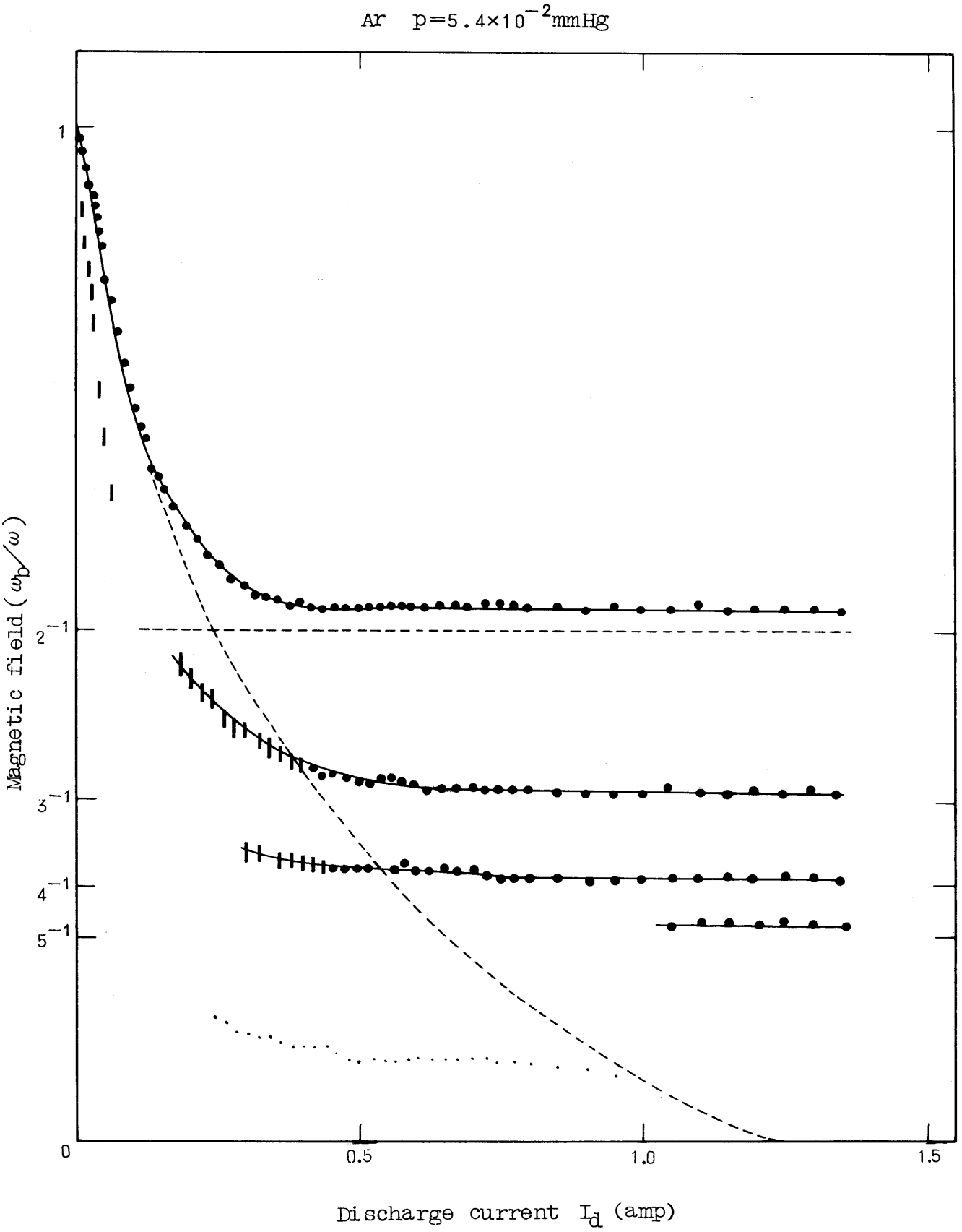
Ar p=5.4×10⁻²mmHg
Magnetic field (ω_b/ω)
1
2⁻¹
3⁻¹
4⁻¹
5⁻¹
0
0.5
1.0
1.5
Discharge current I_d (amp)

Fig. 11

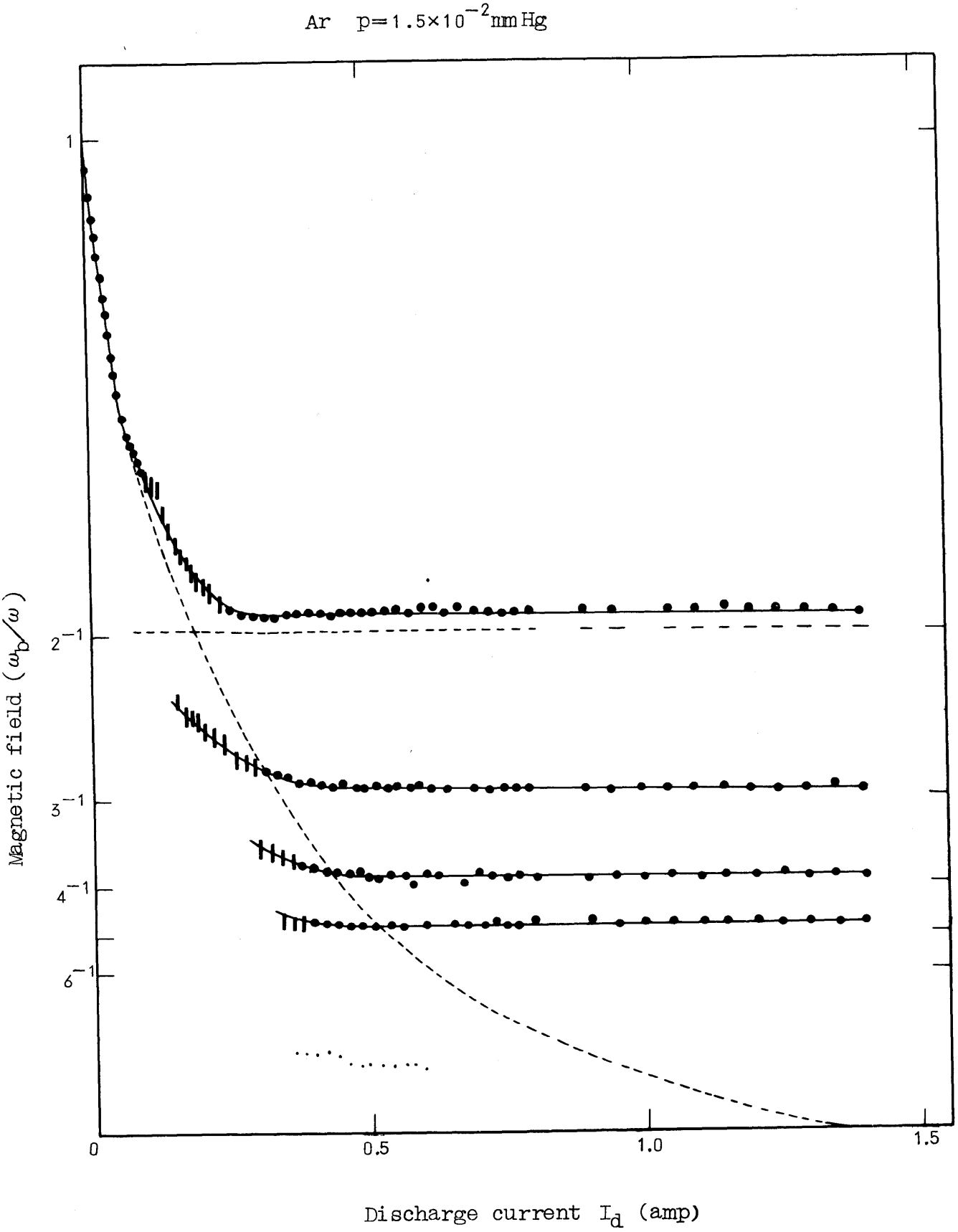
Ar p=1.5×10⁻² mm Hg
1
2⁻¹
3⁻¹
4⁻¹
6⁻¹
0
0.5
1.0
1.5
Magnetic field (ωb/ω)
Discharge current Id (amp)

Fig. 12

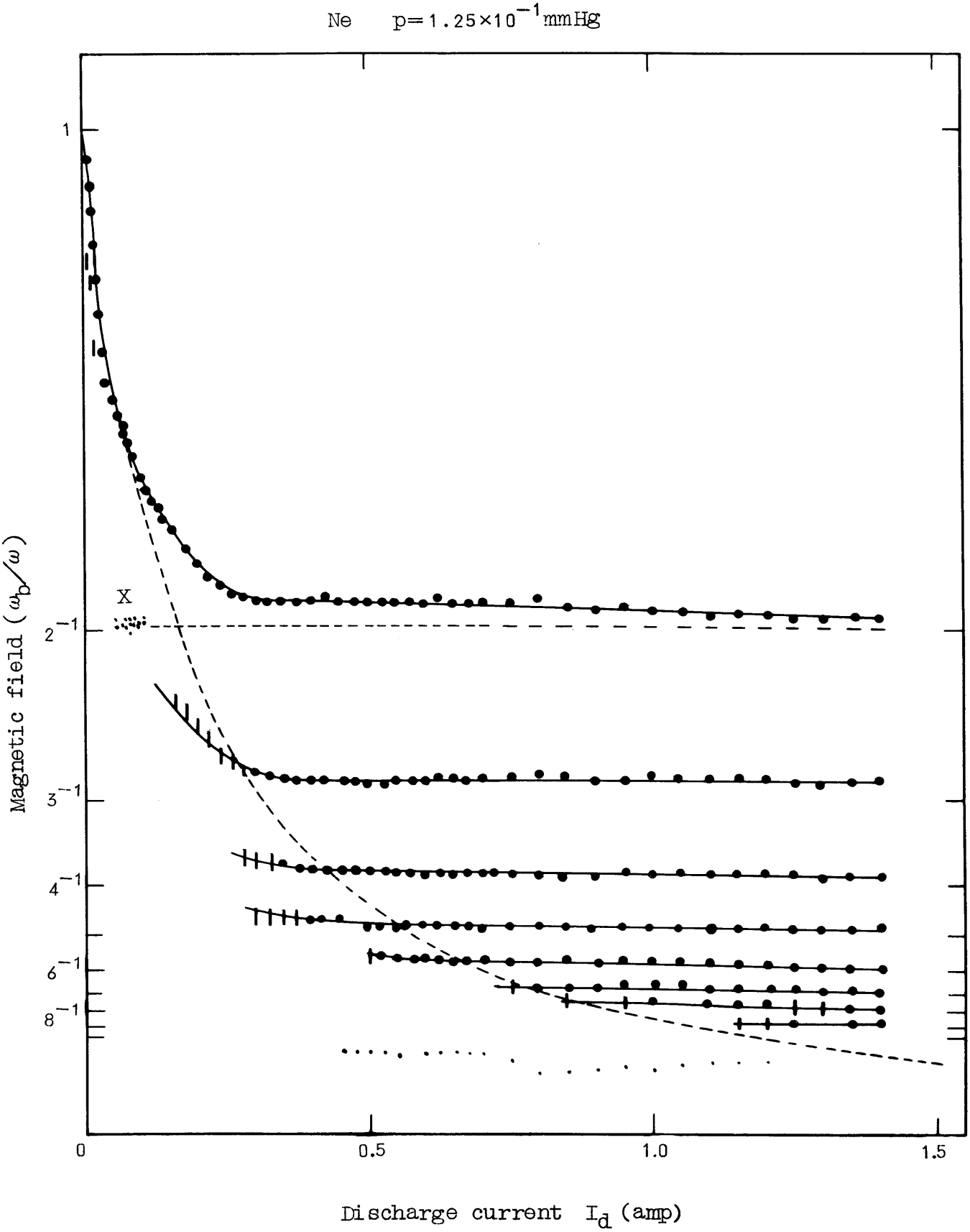
Ne p=1.25×10⁻¹mmHg
Magnetic field (ωp/ω)
1
2⁻¹
3⁻¹
4⁻¹
6⁻¹
8⁻¹
X
0
0.5
1.0
1.5
Discharge current Id (amp)

Fig. 13

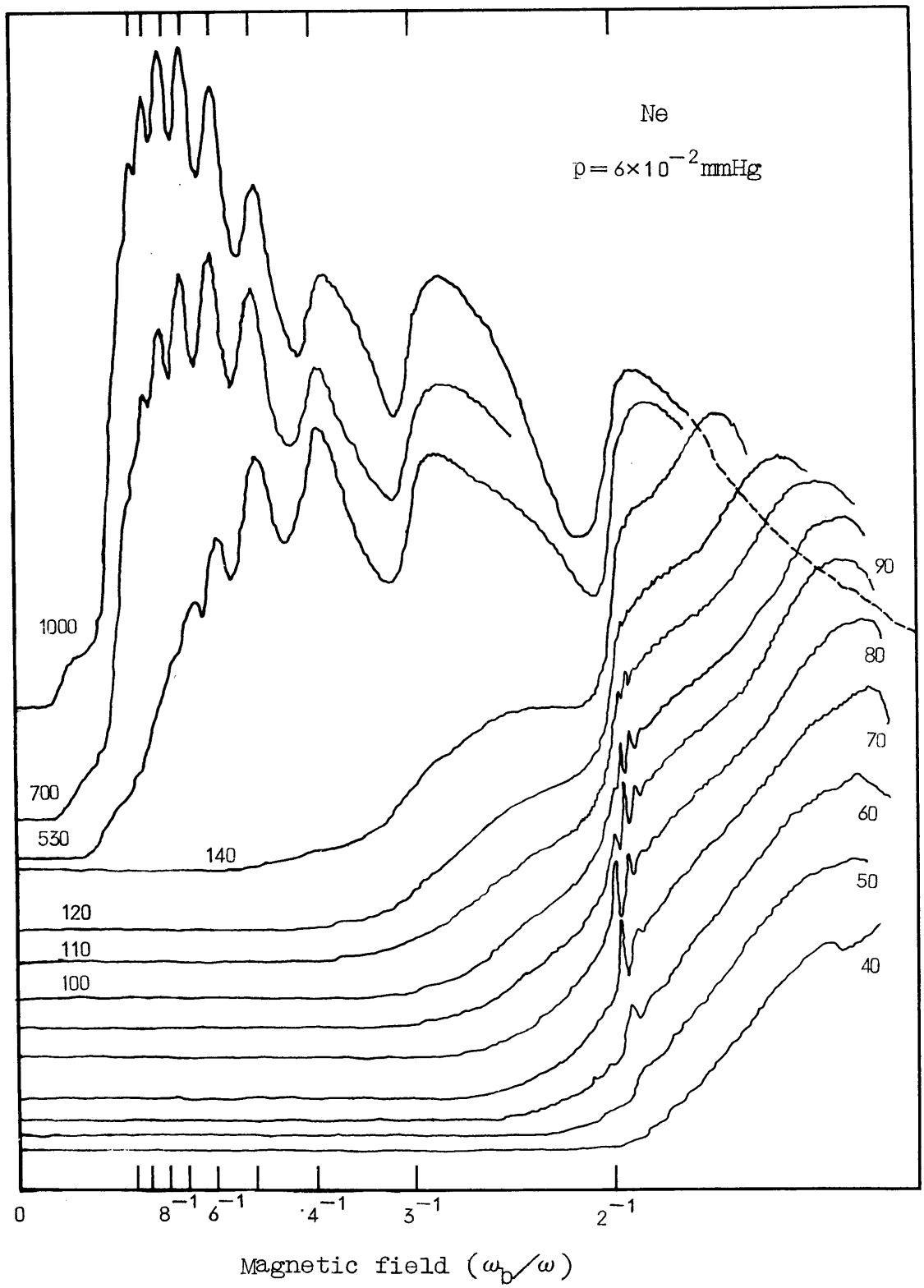
Ne
p = 6×10⁻² mmHg
1000
700
530
140
120
110
100
90
80
70
60
50
40
0
8⁻¹
6⁻¹
4⁻¹
3⁻¹
2⁻¹
Radiated power
Magnetic field (ω_b/ω)

Fig. 14

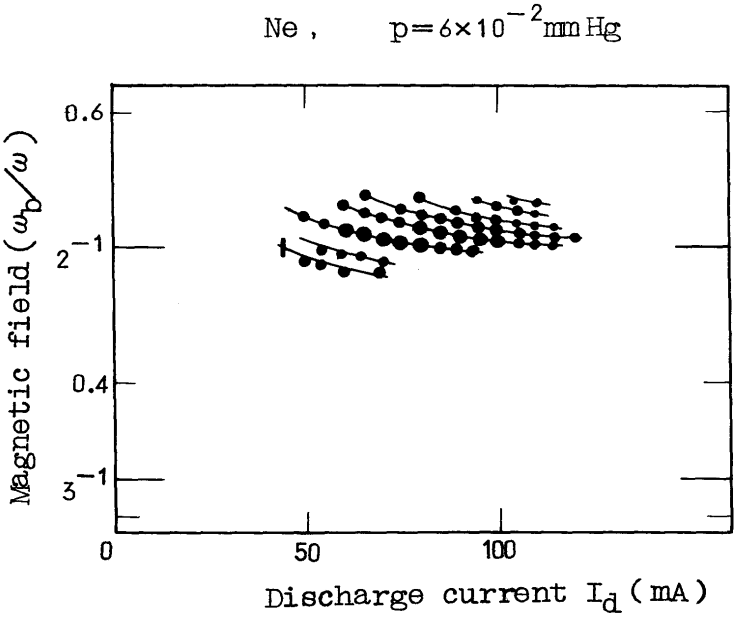
Ne , p=6×10⁻²mmHg
Magnetic field (ωb/ω)
0.6
2⁻¹
0.4
3⁻¹
0
50
100
Discharge current Id (mA)

Fig. 15

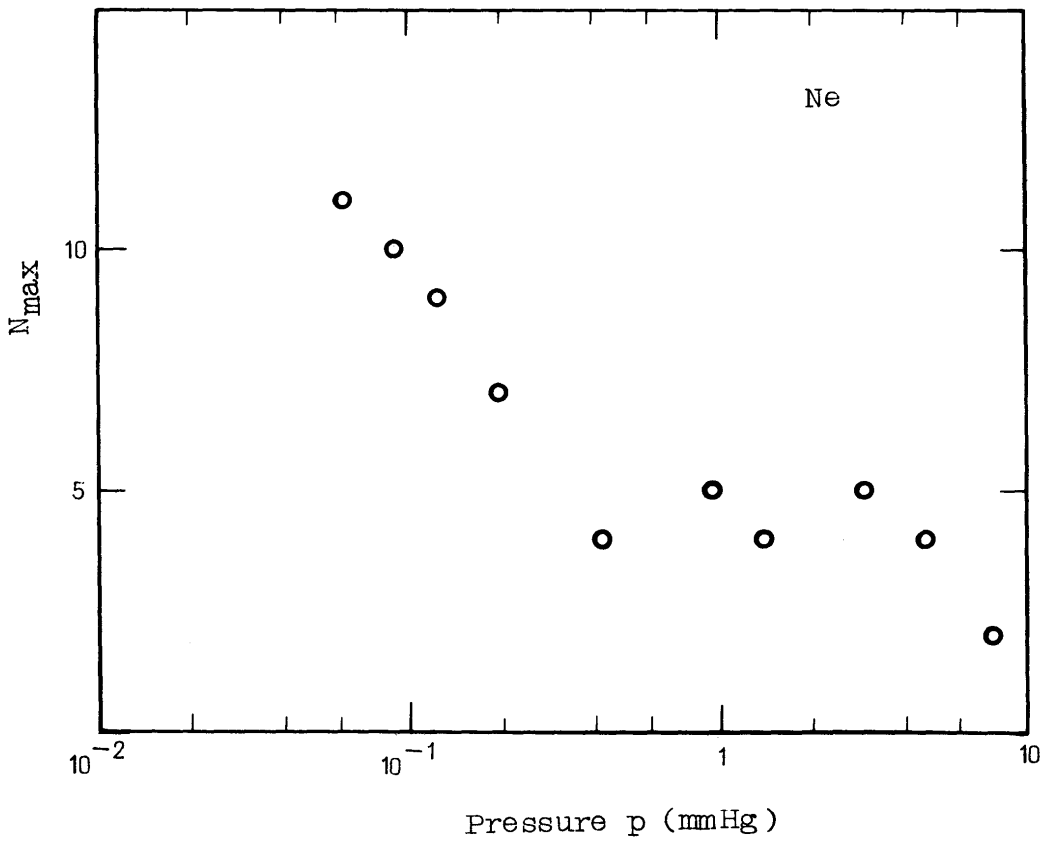
Ne
Nmax
10
5
10⁻²
10⁻¹
1
10
Pressure p (mmHg)

Fig. 16

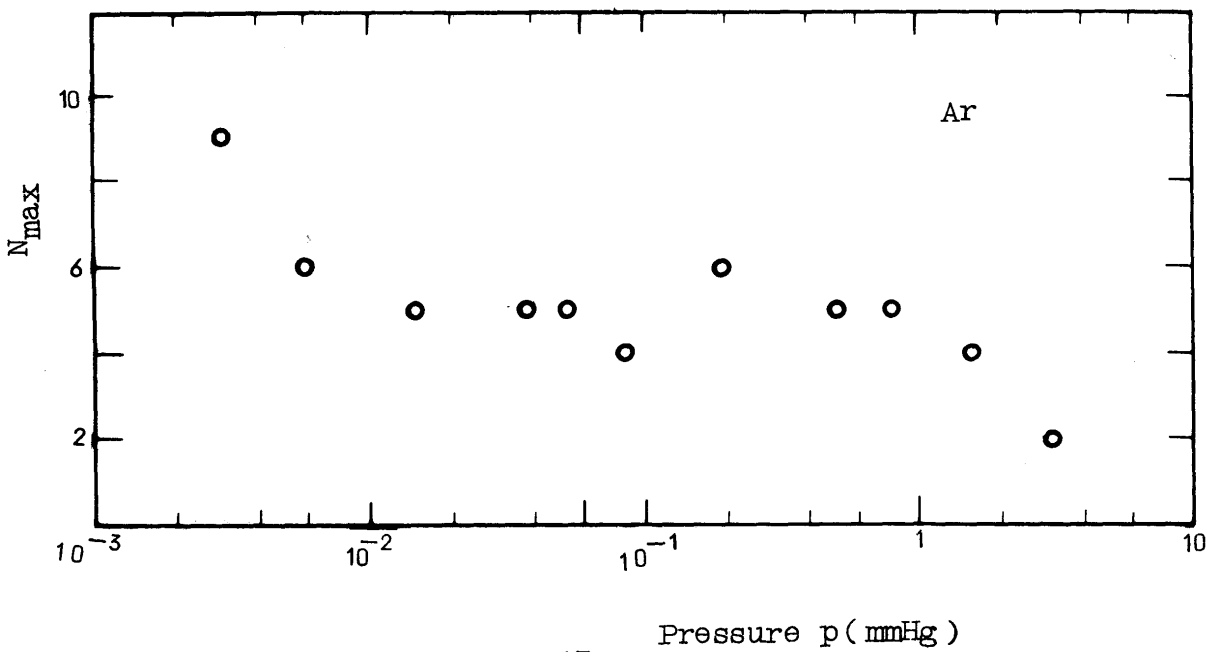
Ar
N_{max}
10
6
2
10^{-3}
10^{-2}
10^{-1}
1
10
Pressure p(mmHg)

Fig. 17

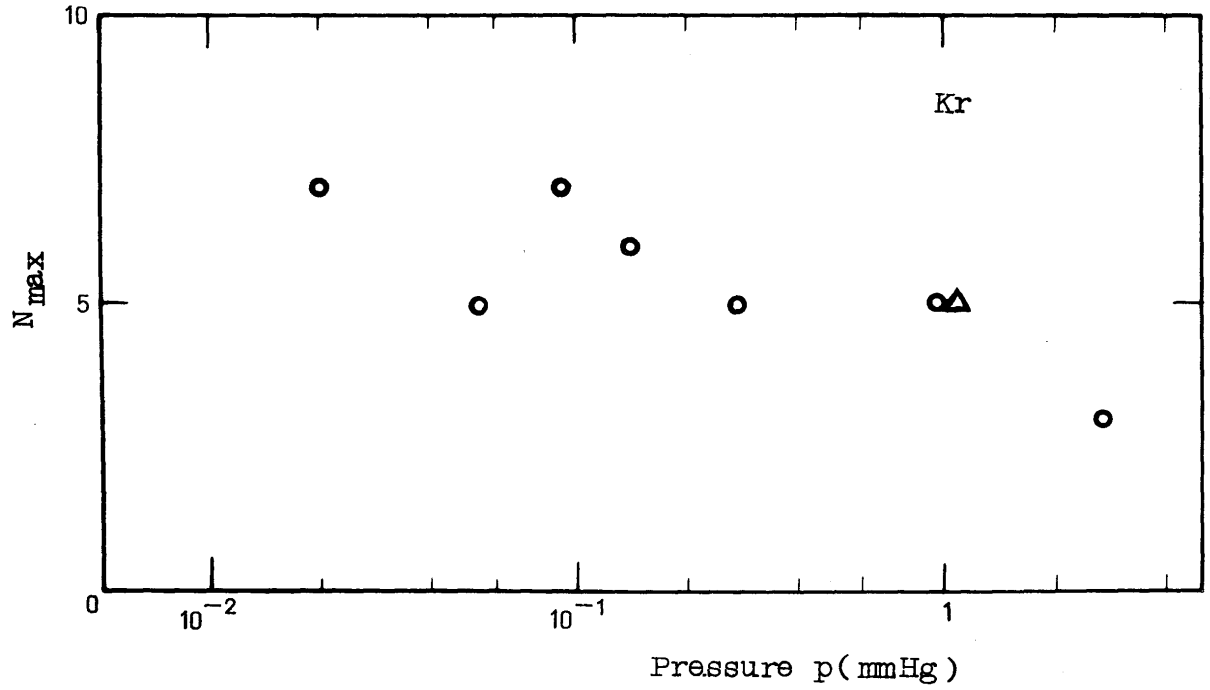
Kr
N_{max}
10
5
0
10^{-2}
10^{-1}
1
Pressure p(mmHg)

Fig. 18

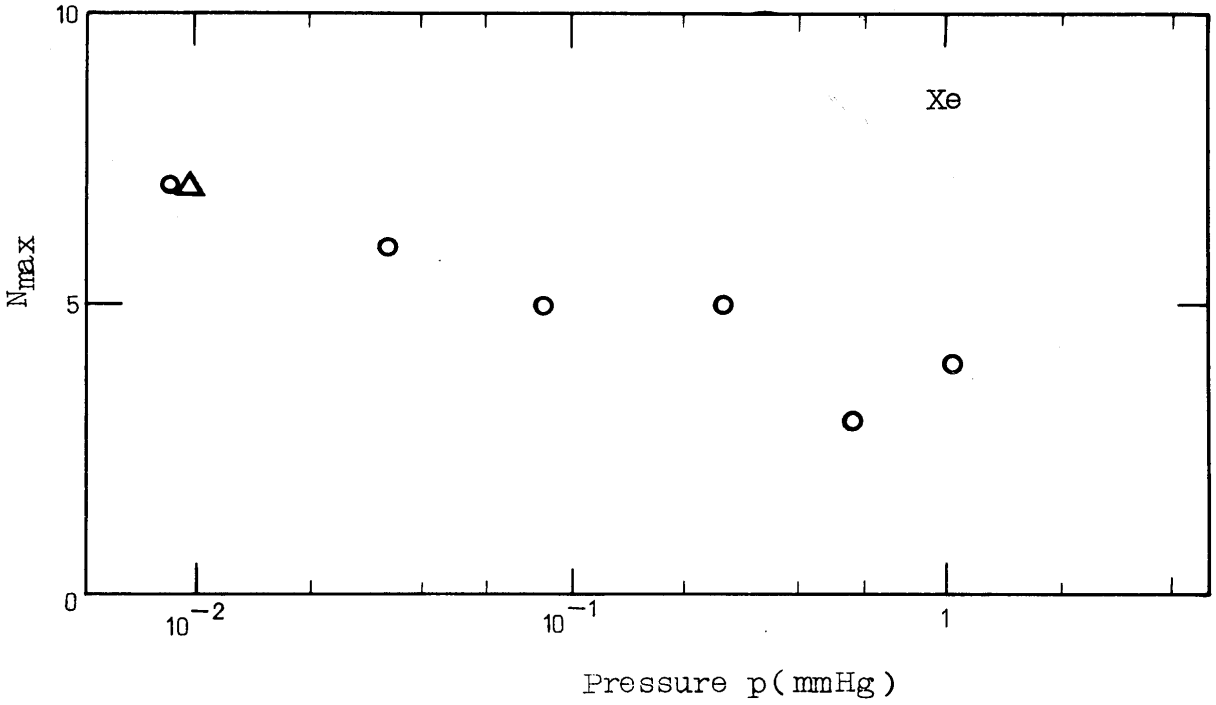

Fig. 19